Detailed Assessment of Compositional and Interfacial Tension Effects on the Fluid Behaviour During Immiscible and Near-Miscible CO_2 Continuous and WAG Displacements

Transport in Porous Media
https://doi.org/10.1007/s11242-019-01368-x

Detailed Assessment of Compositional and Interfacial Tension Effects on the Fluid Behaviour During Immiscible and Near-Miscible CO_2 Continuous and WAG Displacements

Gang Wang[1] · Gillian E. Pickup[1] · Kenneth S. Sorbie[1] · Eric J. Mackay[1]

Received: 28 August 2018 / Accepted: 8 November 2019

Abstract

This study seeks to improve numerical simulations of the key physics occurring in CO_2 enhanced oil recovery (CO_2-EOR) processes, with a particular focus on the transition from immiscible to miscible displacements. In the previous work, we have investigated interactions between compositional effects and the underlying heterogeneities of the flow field in near-miscible floods (Wang et al. in Transp Porous Media 129(3):743–759, 2019a). In this current study, we have further analysed the effects of reduction in interfacial tension (IFT) on the flow behaviour, as motivated by the study on the film-flow mechanism previously presented by Sorbie and van Dijke (SPE improved oil recovery symposium, Society of Petroleum Engineers, 2010). We identify two clear mechanisms of oil recovery that may occur in near-miscible CO_2 (or other gas) injection processes, which we denote, M_{CE}, as oil stripping or conventional compositional effects, and M_{IFT} as lower IFT oil film-flow effects. The latter M_{IFT} effects are described by an enhanced hydrocarbon relative permeability in the near-miscible three-phase relative permeabilities (3PRP). Various combinations between the M_{CE} and M_{IFT} mechanisms were tested by numerical simulations to evaluate the impact of each mechanism on the flow behaviour, i.e. their separate and joint effects on quantities such as the local oil displacement efficiency, phase flow vectors and the ultimate oil recovery. When acting in combination, the oil stripping and IFT effects can greatly improve the local displacement performance even when viscous fingering flow occurs. Viscous fingering is well known to lead to bypassed oil in the "non-preferential" flow paths between the main fingers. We show that the remaining oil in these non-preferential flow paths (i.e. bypassed oil) can be efficiently recovered by the combined M_{CE} and M_{IFT} mechanisms, but only with the application of water alternating gas (WAG). In contrast to oil stripping effects, the IFT effect is not dependent on continuous contact between oil and CO_2. Instead, the remaining oil is mobilized by gas as the IFT is reduced and can be efficiently produced by subsequent water injection. This M_{IFT} mechanism has much less impact in cases with continuous CO_2 injection compared to its efficiency in WAG. This is because during continuous injection, gas fingers are dominant in the preferential flow paths, and therefore the local displacement efficiency is very good, but only in these preferential routes. On the other hand, WAG is able to make full use of the IFT effects because of its relatively stable displacing front, which allows the M_{IFT} mechanism to contribute. In this study, the effects of using different three-phase relative permeability methods were investigated and, as expected, different methods

Extended author information available on the last page of the article

Published online: 19 November 2019

yielded different results. However, an important observation is that when IFT effects (M_{IFT}) were included, there was much less difference in the final oil recovery using the different 3PRP models; our analysis shows why this is the case.

Keywords Interfacial tension effects · Compositional effects · Near-miscible displacements · CO_2 WAG · Fingering flow

List of Symbols

f	Weighting factor for IFT effects
K_{rg}	Gas relative permeability
K_{rgt}	Total gas relative permeability (under IFT effects)
K_{rh}	Miscible hydrocarbon relative permeability
K_{ro}	Oil relative permeability
K_{rot}	Total oil relative permeability (under IFT effects)
K_{rw}	Water relative permeability
M_{CE}	Oil stripping effects
M_{IFT}	Interfacial tension effects
n	Exponent of the equation for weighting factor
S_g	Gas saturation
S_o	Oil saturation
S_{org}	Residual oil saturation to gas
S_{orw}	Residual oil saturation to water
S_w	Water saturation
S_{wc}	Connate water saturation
PVI	Pore volume injection
σ_{go}^0	Threshold value at which IFT effects are triggered
σ_{go}	Interfacial tension between oil and gas

1 Introduction

As CO_2 is injected into an oil reservoir, a set of mutual interactions between in situ oil and the injected CO_2 start to occur. CO_2 dissolves into oil, and oil components are vaporized until a local equilibrium is achieved (Stalkup 1983; Orr 2007). Both saturations and properties of flowing phases are dynamically changed throughout the whole process. For this reason, it is very challenging to properly model and predict such cases due to the complexity of multiphase flow and the process of mass transfer (described by a PVT model, such as an equation of state, EOS). In this work, we refer to this stripping/compositional process as Mechanism 1 (M_{CE}). As the pressure increases and the system comes closer to miscibility, a situation we describe as "near-miscible", another oil recovery mechanism involving enhanced oil layer flow occurs. Sorbie and van Dijke (2010) cited both experimental observations and presented theoretical evidence that significant hydrocarbon film/layer flow occurs at gas/oil IFT (σ_{go}) above miscibility, i.e. $\sigma_{go} \sim 1$–3 mN/m. This is referred to as Mechanism 2 (M_{IFT}), and it manifests itself as an increase in hydrocarbon relative permeability in the near-miscible three-phase relative permeability (hereafter denoted as 3PRP).

At low pressures, CO_2 flooding may increase oil recovery by oil swelling and viscosity reduction (Green and Willhite 1998). As pressure increases, CO_2 starts to become miscible with oil (multicontact-miscible) and two mechanisms become important for enhancing

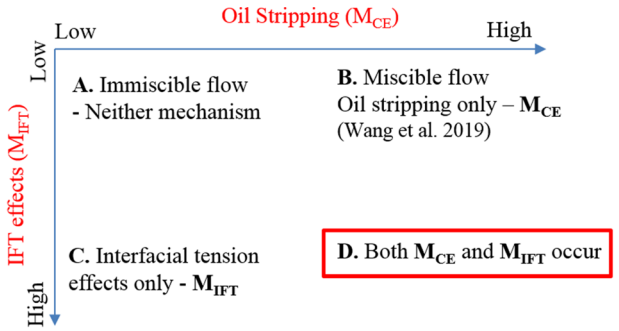

Fig. 1 Schematic of the possible mechanistic processes that may occur in a CO_2 (gas) displacement process at immiscible and near-miscible conditions. Note that the pressure increases from left to right along the horizontal axis, and from top to bottom along the vertical axis

oil displacement: compositional effects (oil stripping) and low interfacial tension (IFT) effects (Amaefule and Handy 1982; Shyeh-Yung 1991; Juanes et al. 2006). When multicontact miscibility occurs and oil components are vaporized into CO_2 (and thus are in the "gas" phase), the lighter components are vaporized first, and the oil components are spread out, similar to chromatography (Zick 1986; Orr 2007). At the same time, interfacial tension between gas and oil (σ_{go}) can also be greatly reduced due to component transfer. As a result, the relative permeability for a simple oil may become linear as the system achieves miscibility under certain conditions. We will show that full miscibility is rarely reached with more complex oil in CO_2/WAG simulations, but this is not an impediment to very efficient combined M_{CE}/M_{IFT} oil displacement mechanisms. Figure 1 shows a schematic diagram with the range of possible mechanistic combinations (M_{CE} and M_{IFT}) that can occur (at least theoretically) in CO_2 (or other gas) displacement processes.

In the previous work (Wang et al. 2019a), we presented a detailed numerical study on the compositional effects and their influencing factors for this single mechanism (M_{CE}). The goal of this study is to address the distinction between these two mechanisms, M_{CE} and M_{IFT} (IFT relative permeability effects), on the flow behaviour in heterogeneous permeability fields. A further motivation for this study is to analyse the overall outcome when these mechanisms are incorporated within the most widely used models describing 3PRP, such as Stone 1, Stone 2 and Baker's saturation-weighted method (Aziz and Settari 1979; Baker 1988). We believe that this detailed analysis of the modelling process of the oil displacement by CO_2 at near-miscible conditions within fine-scale models will lead to the development of more rigorous ways to simulate large-scale CO_2-EOR processes. The complete data set and results of this study are available online as a model case example for testing potential upscaling techniques for compositional flows in heterogeneous systems. The DOI for this supplementary material is https://doi.org/10.17861/fc1c90bb-9d3f-4a6c-9170-7b7fe10ec7b9.

2 Literature Review

Longeron (1980) and Bardon (1994) performed a series of core flooding tests to investigate the IFT effects on relative permeability using a binary fluid mixture. They concluded that the residual oil saturation is highly dependent on the value of IFT between gas and oil,

especially when it is lower than 0.1 mN/m. Very importantly, the relative permeabilities to both oil and gas became linear as IFT approached zero. This is a very important result in the literature on near-miscible gas injection, but it omits the effects of the presence of much heavier hydrocarbon components in real oils. For such realistic systems, the stripping/compositional effect removes the lighter components leaving the heavier ones behind and as the displacement progresses, the gas/oil IFT will frequently increase, as we show here.

Coats (1980) developed a comprehensive compositional model to simulate gas displacement taking account of both compositional effects and IFT effects. The implicit formulation used in his study is particularly efficient for multi-contact-miscibility systems, such as oil displacement by CO_2. Coats' simulations suffered from numerical dispersion, because he had limited computer power, but his method of modelling compositional problems has been widely applied since then and has been coded in commercial software, namely Eclipse 300 (Schlumberger 2015).

Zick (1986) investigated experimentally and numerically the process of mass transfer during the enriched-gas displacement. He demonstrated in detail how the combined mechanism of vaporizing/condensing makes the enriched-gas displacements very efficient, even if the true miscibility is not achieved. Tang and Zick (1993) summarized the advantages and flaws of typical conventional four-component simulators, such as composition-independent *K*-value models, solubility models and chase gas models. Very importantly, they pointed out the necessity of a fully compositional simulator (EOS based) to properly model the near-miscible CO_2 displacement.

Baker (1988) made a thorough review of the 3PRP models which had been published at that time. Since none of them was able to make a sufficiently good prediction of the experimental data, he proposed the saturation-weighted and linear interpolation methods, with the aim of improving the fit to experimental results. Since his methods generally provided a better fit to the data available at that time, the saturation-weighted model has been implemented in Eclipse as the default method to calculate 3PRP (Schlumberger 2015).

Betté et al. (1991) performed a series of numerical simulations to evaluate IFT effects on fluid behaviour. They claimed that IFT effects barely affect the ultimate recovery. In fact, the IFT effects in their study were probably masked by the more dominant compositional effects. They only simulated continuous injection of CO_2 into 1D slim-tube models and cores, and they did not simulate WAG. Although the importance of IFT effects was not well resolved, their method of simulating IFT effects has been well accepted and incorporated in commercial software, namely GEM/CMG (CMG 2017). This present work agrees with the finding of Betté et al. for continuous gas injection, but we go on to show that IFT effects are much more important in near-miscible WAG processes.

Blunt (2000) proposed an empirical model for 3PRP to improve Baker's method. He addressed the importance of layer drainage on the prediction of oil relative permeability at low oil saturation. He stated that zero residual oil may be more appropriate when gas injection is involved, and this limit might be reached gradually by oil film (layer) flow.

Sohrabi et al. (2004, 2008a, b) designed a series of capillary-dominated WAG tests to evaluate IFT effects at the pore scale. They used etched glass micromodels to mimic the pore structure of reservoir rocks and varied the wettability conditions by injecting either water or oil before the tests. They claimed that if the IFT between oil and gas is reduced to the level of 1–3 mN/m, good oil recovery can be obtained through either a thick oil film (oil wetting) or an oil layer (water wetting). In other words, the local displacement efficiency can be greatly improved by means of an "oil film", even though the IFT is not at an ultra-low level (i.e. $\sigma_{go} \sim 1$–3 mN/m and not necessarily as low as $\sigma_{go} \sim 0.001$ mN/m).

Sorbie and van Dijke (2010) proposed a consistent pore-scale theory of phase flow for the transition from immiscible to miscible conditions with respect to the impact of IFT effects on the contact angles. They modified the equations for the pore-scale model, originally proposed by Al-Siyabi et al. (1999) to account for this low-IFT (but not ultra-low) transition. They concluded that the "oil film" mechanism is particularly important during near-miscible WAG, where IFT could be reduced to 1–3 mN/m; this would normally be described as "immiscible", but is better described as "near-miscible". In the simulations described below, we therefore suppose that the increase in relative permeability with decreasing IFT is related to this "oil film" mechanism (M_{IFT} in Fig. 1), although the simulator simply represents it as an enhanced oil-phase relative permeability.

In a recent paper, Jahanbakhsh et al. (2018) compared the IFT effects on relative permeability of all three phases between immiscible and near-miscible WAG. They concluded that both oil and gas relative permeability could increase with decreasing IFT and therefore the oil recovery is significantly improved. However, they did not explicitly differentiate the oil recovery mechanisms between the low-IFT effect and the oil stripping effect.

The above review is presented to put the current study into the context of earlier work, which is mostly focused on the simulation of CO_2 displacement, particularly under near-miscible conditions. Our survey of the literature indicates that many aspects of the modelling of flow behaviour under low-IFT effects (but not ultra-low) have not been fully investigated, particularly when compositional effects (M_{CE}), IFT effects (M_{IFT}), heterogeneities and multiphase flow are all involved, such as during near-miscible CO_2 WAG.

3 Methodology

3.1 Modelling of Interfacial Tension Effects

The modelling of interfacial tension effects is carried out utilizing the gas/oil relative permeability model implemented in CMG/GEM (CMG 2017). This model is specified by Eqs. 1–4 below and is based on the Coats' model (Coats 1980; Betté et al. 1991). This method entails an interpolation between immiscible (initial) and miscible hydrocarbon relative (K_{rh}) permeabilities, with the use of a weighting function (f). A critical gas/oil IFT, σ^0_{go}, is specified. If the actual σ_{go} (calculated by the simulator as part of the compositional simulation using the McLeod-Sugden equation) is above the threshold value (σ^0_{go}), IFT reduction will not have any impact on the flow behaviour. If $\sigma_{\mathrm{go}} < \sigma^0_{\mathrm{go}}$, the relative permeability of oil and gas will be modified to K_{rot} and K_{rgt}, respectively, with these gradually becoming linear functions as σ_{go} approaches zero. As seen in Eq. 4, the smaller the weighting factor (f), the greater the impact IFT effects will have on the relative permeabilities. The exponent "n" involved in Eq. 4, which is normally from 0.1 to 0.5 (Coats 1980), was set to 0.5 here.

$$K_{\mathrm{rot}} = f * K_{\mathrm{ro}} + (1-f) * K_{\mathrm{rh}} * \left(S_{\mathrm{o}} / \left(1 - S_{\mathrm{w}}\right)\right) \tag{1}$$

$$K_{\mathrm{rgt}} = f * K_{\mathrm{rg}} + (1-f) * K_{\mathrm{rh}} * \left(S_{\mathrm{g}} / \left(1 - S_{\mathrm{w}}\right)\right) \tag{2}$$

$$\begin{aligned} &K_{\mathrm{rh}} = 0.5 * \left(K_{\mathrm{row}} + K_{\mathrm{rg}}\right) \\ &\text{where } f = 1, \quad \text{if } \sigma_{\mathrm{go}} > \sigma^0_{\mathrm{go}} \end{aligned} \tag{3}$$

$$= (\sigma_{go}/\sigma^0_{go})^n, \text{ otherwise} \tag{4}$$

3.2 Fluid Property and Relative Permeability

An example of light oil with a minimum miscibility pressure (MMP) of 120 bar and a viscosity of 0.16 mPa s was used in our study. The bubble point pressure was 38.5 bar at 53 °C. The full fluid data used for the generation of a Peng–Robinson equation of state can be found in our previous paper (Wang et al. 2019a). In fact, we attempted to lump this seven-component oil into four components (CO_2, CH4, C2-7 and C8+) to reduce the compositional cost. However, the four-component system exaggerates the compositional effects and "film-flow mechanism" (see "Appendix") if we only use one component to control almost half of the oil composition (45.6% here). In order to guarantee the consistent process of mass transfer, a seven-component system with more detailed definition of heavy components was used in our study.

The oil/water and oil/gas two-phase relative permeability curves used here are shown in Fig. 2. Note that a relatively high S_{org} (to immiscible gas displacement) is chosen here ($S_{org}=0.33$) to give a higher target oil for IFT reduction effects, with the aim of emphasizing the magnitude of effects occurring in the transition from immiscible to miscible conditions on the ultimate oil recovery. As the IFT decreases, the gas–oil relative permeability becomes linear. Here, we present examples of relative permeability varying the ratio, $\sigma_{go}/\sigma^0_{go}$ (local grid IFT over threshold value), using the relative permeability model defined by Eqs. 1–4. This is shown in Fig. 3, for the gas–oil relative permeability depicted in the right side of Fig. 2.

Since the oil isoperm could be greatly biased by the choice of 3PRP model, a sensitivity analysis on 3PRP methods such as the Stone 1 and 2 models (Aziz and Settari 1979) and Baker's saturation-weighted interpolation (Baker 1988) was conducted to investigate the overall outcome of the two near-miscible displacement mechanisms discussed above (M_{CE} and M_{IFT}) when WAG is applied.

3.3 1D Slim Tube

In order to determine the threshold value (σ^0_{go}), 1D numerical slim-tube simulations (near miscible and immiscible) were performed to track the interfacial tension between

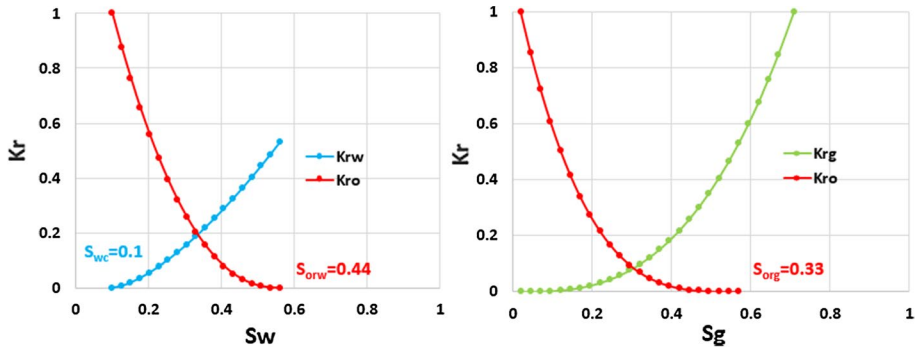

Fig. 2 Oil–water and oil–gas relative permeability curves

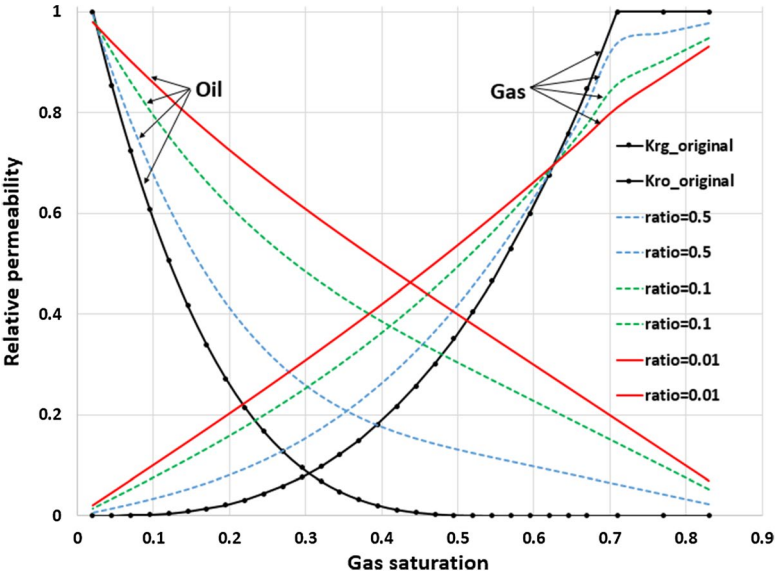

Fig. 3 Relative gas and oil permeability of an example with varying (σ_{go} / σ^{0}_{go}) ratio

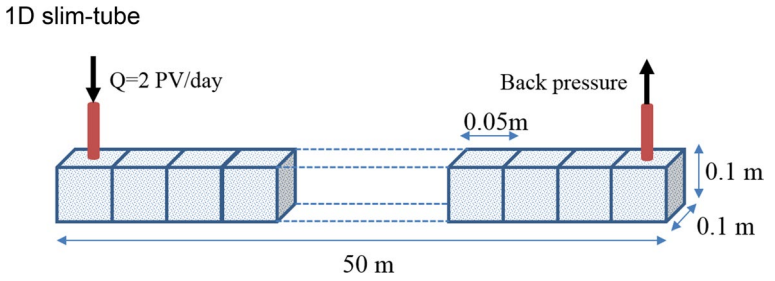

Fig. 4 Schematic of numerical slim-tube test

oil and gas (σ_{go}) during the whole injection process. As seen in Fig. 4, the length of the slim-tube model here (50 m) was longer than a conventional slim tube to reduce the possible fluctuations in the numerical results. More importantly, the results achieved in 1D tests can be directly compared to the subsequent 2D tests with the same "well spacing".

3.4 2D Areal Heterogeneous Model

A small 50 m × 10 m ($\Delta x = \Delta y = 0.05$m) heterogeneous permeability field was generated with a Dykstra-Parsons (V_{DP}) coefficient of 0.7 (Dykstra and Parsons 1950) and dimensionless correlation range (R_L) of 0.1 (Journel and Huijbregts 1978). This model of the permeability field, which is effectively the size of a single grid block in a full field model, is shown in Fig. 5. With a relatively short correlation length ($R_L \sim 1/10$ of system length), this field was chosen to trigger possible fingering flow. Both wells were horizontal and were perforated along the width of the model. The injector in our tests was set to inject displacing

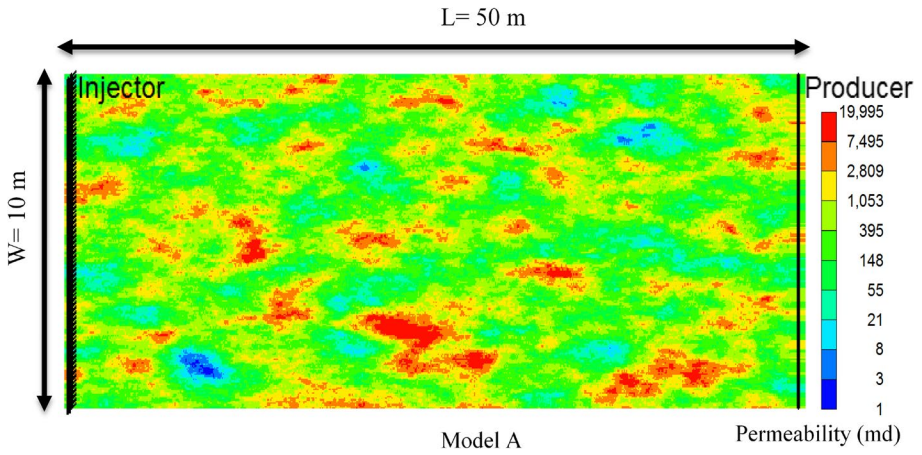

Fig. 5 Permeability field A ($V_{DP}=0.7$, $R_L=0.1$) used to trigger fingering flow

Table 1 Injection strategy

Continuous injection (1 PVI in total)	1 PVI continuous CO_2 injection at reservoir conditions				
WAG injection (2 PVI in total)	First water cycle	First gas cycle	Second water cycle	Second gas cycle	Third water cycle
	0.4 PVI water	0.4 PVI CO_2	0.4 PVI water	0.4 PVI CO_2	0.4 PVI water

fluid at a rate of 0.4 PV/d, and the producer was controlled by setting the minimum bottom-hole pressure. Both continuous CO_2 injection and WAG injection were modelled to investigate both the compositional and the IFT effects on the flow behaviour and the ultimate oil recovery with different injection methods. The injection strategy was designed to represent the flow behaviour of interest, such as fingering flow, improvement of sweep by water and the ultimate distribution of residual oil (Table 1).

4 Results and Discussions

4.1 1D Slim Tube: 1 PVI Continuous CO_2 Injection at Immiscible Conditions (70 bar)

The first set of simulations studied IFT effects (M_{IFT}), in the absence of compositional effects (M_{CE}). This is an artificial scenario, but is useful for gaining an understanding of IFT effects. The simulations were performed at a pressure of 70 bar, which was below the minimum miscibility pressure (MMP). In order to determine the threshold value of σ_{go}^0 and therefore properly model the IFT effects, a representative cell (3/10 of the 1D system length from the slim-tube injector) was selected to track its IFT throughout the whole process of immiscible displacement. As shown in Fig. 6, IFT first decreases from 7 to 3 mN/m and then increases again up to about 5 mN/m. In fact, we might expect some degree of IFT effects (Mechanism M_{IFT}) to occur in this lower IFT range, if, for example, the σ_{go}^0 in the IFT model was set to, say, $\sigma_{go}^0=5$ mN/m. However, to illustrate the effects of the IFT

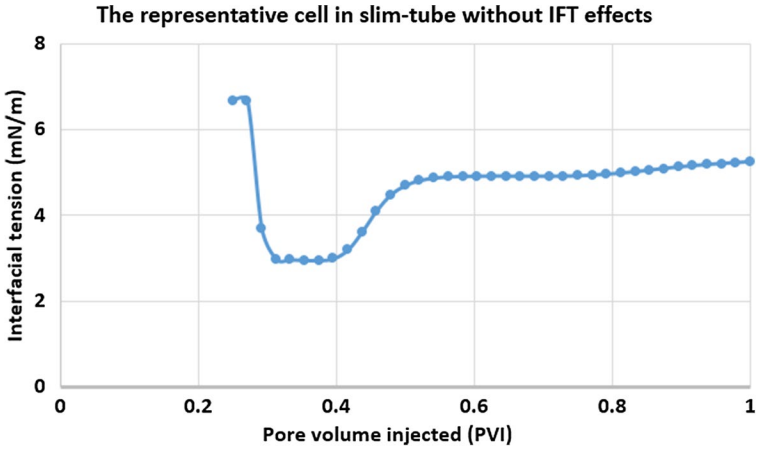

Fig. 6 IFT in the representative cell at immiscible conditions

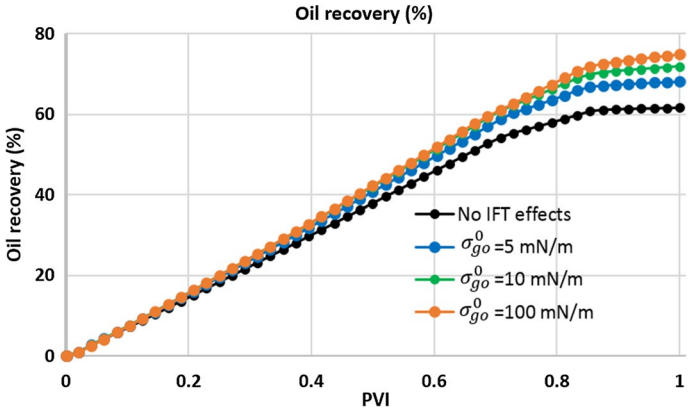

Fig. 7 Recovery factor from cases varying the threshold value, σ^0_{go}

only in this immiscible displacement, we tested a range of threshold values (from 5 to 10 mN/m) to analyse its effects on the ultimate oil recovery. In addition, we set the threshold to 100 mN/m in order to examine an extreme (non-physical) case where the IFT effect is "switched on" throughout the displacement rather than only in the notional "near-miscible" region. Oil recovery results are shown in Fig. 7 for various σ^0_{go}. Thus, we are simulating the immiscible displacement to minimize the compositional effects, but emphasize the IFT effects through testing a set of larger threshold values.

Results in Fig. 7 show, as expected, that the greater the value of σ^0_{go}, the better the ultimate oil recovery. More importantly, it is found that even with the threshold value of 100 mN/m (the IFT effects act under *all* conditions in the displacement), the ultimate oil recovery is 76%, which is much less efficient than a typical near-miscible slim-tube flood (generally close to 90%).

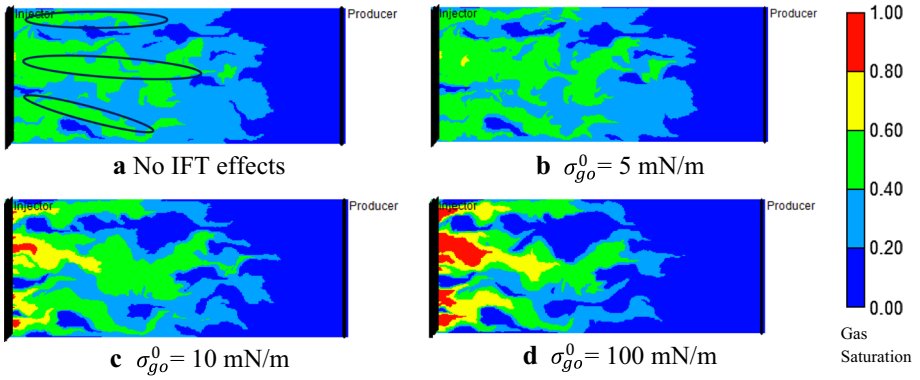

Fig. 8 Gas saturation with 0.5 PVI of CO_2 at immiscible conditions

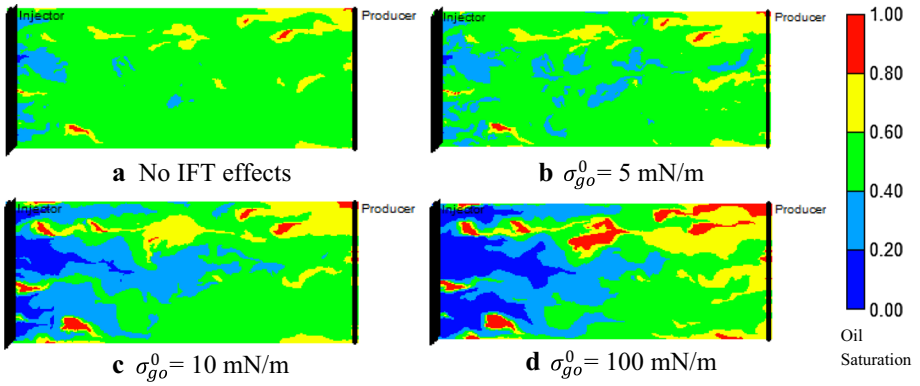

Fig. 9 Remaining oil saturation after 1 PVI immiscible displacement

Fig. 10 Oil recovery varying the threshold value at immiscible conditions after 1PV CO_2 continuous injection

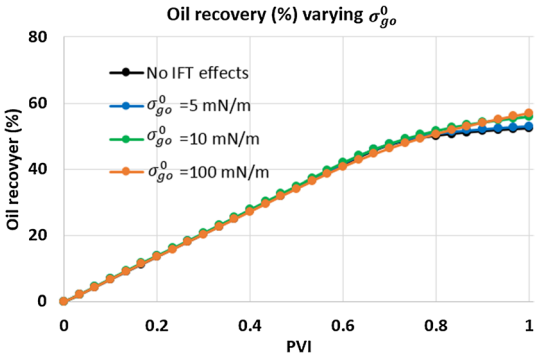

4.2 2D Areal Test: 1 PVI Continuous CO_2 Injection at Immiscible Conditions (70 bar)

In order to evaluate the significance of IFT effects when viscous instability and heterogeneity are involved, σ^0_{go} was set to 5, 10 and 100 mN/m for the subsequent 2D areal immiscible CO_2 displacement. Therefore, the smallest ratios of $\sigma_{go}/\sigma^0_{go}$ are about 0.6, 0.3 and 0.03, respectively. Note that σgo is not constant throughout the injection process due to component mass transfer, which is weak at immiscible conditions but strong at near-miscible conditions.

Figure 8 shows the fluid distributions after 0.5PV of CO_2 injection under purely immiscible (no IFT) conditions, and with IFT effects for the three values of $\sigma^0_{go}=5$, 10 and 100 mN/m. As expected, fingering flow occurs in the system due to the unfavourable mobility ratio. For the same amount of CO_2 injection at reservoir conditions, cases with increasing IFT threshold value show decreasing macroscopic sweep efficiencies. The oil mobilized by IFT effects can then be recovered allowing more gas to flow into these regions. The consequent higher gas saturation leads to more aggressive gas fingers and therefore aggravates the imbalance of the fluid flow between "preferential routes" in the gas fingers (as indicated by oval shapes in Fig. 8) and "non-preferential" bypassed routes. As a consequence, the results in Fig. 9 show that the oil in the non-preferential routes is even more poorly recovered (i.e. bypassed) than the base case (no IFT effects), whereas the oil in the preferential routes can be more efficiently produced. The final result of the competing IFT effects of poorer sweep but lower residual oil in the preferential paths leads to a modest ultimate oil recovery improvement with increasing threshold IFT value (i.e. as σ^0_{go} increases), as shown in Fig. 10.

4.3 1D Slim Tube: 1 PVI Continuous CO_2 Injection at Near-Miscible Conditions (120 bar)

In the previous section, we presented simulations which minimized the oil stripping effects but exaggerated the IFT effects on the flow behaviour in a fingering flow regime. This gave us a better understanding of the magnitude of the impact which IFT effects might have on flow behaviour. Now, we simulate near-miscible displacement ($P=120$ bar) and test varying levels of IFT effects to investigate the combined outcome from both mechanisms (M_{CE} and M_{IFT} shown in Fig. 1). Figure 11 shows the calculated grid block IFT throughout the 1D slim-tube simulation in a representative cell for the near-miscible displacement; the immiscible IFT values from Fig. 6 are also shown for a comparison. Note that IFT effects were switched off in this simulation (with $P=120$ bar), as they were for the one at 70 bar.

As shown in Fig. 11, near-miscible flooding clearly leads to a much wider range of IFT values during the whole process (from 0.01 to 7 mN/m), compared with the previous immiscible displacement. This is, of course, very well known from conventional compositional simulations. In the early stages of the displacement, CO_2 and oil are approaching miscibility through the mass transfer process, and IFT sharply decreases. With further contacts between CO_2 and oil, σ_{go} again increases and the fluids become immiscible. This is because the light–medium oil components have been mostly vaporized leaving the remaining oil consisting mainly of heavy components. This phenomenon is well known and is extensively described in the literature (Orr 2007; Wang et al. 2019a). However, whereas in conventional compositional simulation, this change in IFT is a consequence of the compositional effects (M_{CE}), here it also triggers the near-miscible relative permeability effects (M_{IFT}) as soon as $\sigma_{go}<\sigma^0_{go}$. In addition, these effects lead to a further complexity as they

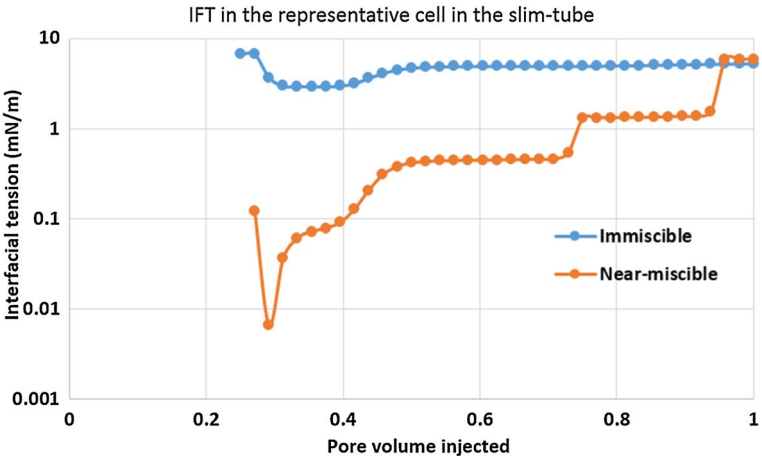

Fig. 11 IFT in the representative cell at near-miscible conditions

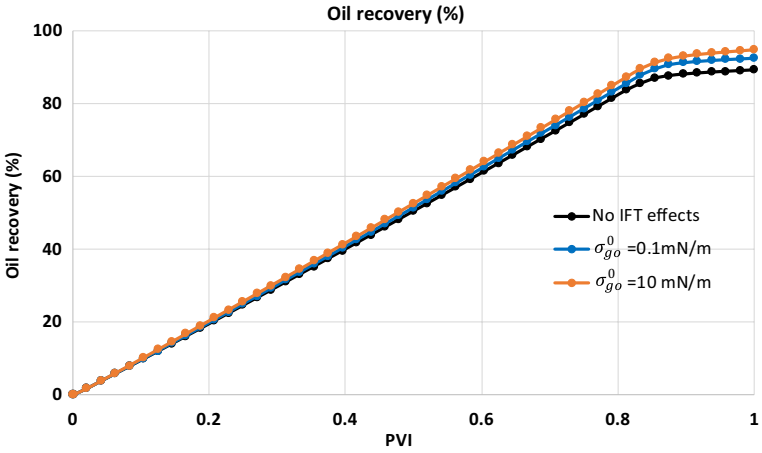

Fig. 12 Recovery factor vs time for various values of σ^0_{go} in the 1D model, near-miscible case

must also interact with the flow behaviour in heterogeneous systems in the preferential and non-preferential flow paths. We demonstrate below that different mechanisms work in different places for different processes.

Again, we tested a range of σ^0_{go} values to analyse the effects of Mechanism M_{IFT} on the oil recovery in the near-miscible 1D oil displacements by CO_2. The IFT effects on the near-miscible displacement in the slim-tube model were found to be minor regarding the oil recovery (see Fig. 12). This is simply because the oil stripping effects have already been able to recover most of the oil in the slim tube in a 1D system. Therefore, there is little target oil saturation for IFT effects to work on. At the same time, the remaining oil saturation mostly consists of the heavy components (higher viscosity) with very poor mobility (which also leads to the increasing IFT as the flood progresses). This will further hinder the oil-phase flow, leading to a fairly limited incremental oil recovery.

4.4 2D Areal Test: 1 PVI Continuous CO_2 Injection at Near-Miscible Conditions (120 bar)

According to Sohrabi et al. (2004) and Sorbie and van Dijke (2010), layer drainage is likely to be an important flow mechanism during near-miscible gas displacement. They found that although gas–oil interfacial tension is not ultra-low (e.g.at a level of 1–3 mN/m), significant oil flow can still be observed through layer drainage. In order to evaluate the significance of such effects, the threshold IFT, σ^0_{go}, in our simulations is set to 3, 5 and 10 mN/m for the following 2D areal near-miscible CO_2 displacements. That is, we now investigate the effect of combined mechanisms (M_{CE} and M_{IFT}) on the flow behaviour, when viscous instability and heterogeneity are involved.

Figure 13 shows the gas saturation distribution in the system after 0.5 PV of CO_2 injection, and Fig. 14 shows the final remaining oil distribution after 1PV of CO_2 injection; the cases shown are for the near-miscible case with $\sigma^0_{go} = 3$, 5 and 10 mN/m. How the oil stripping mechanism affects the flow behaviour can be seen by comparing the results in Fig. 8a with those in Fig. 13a. For the same pore volume of CO_2 injected, the gas saturation is

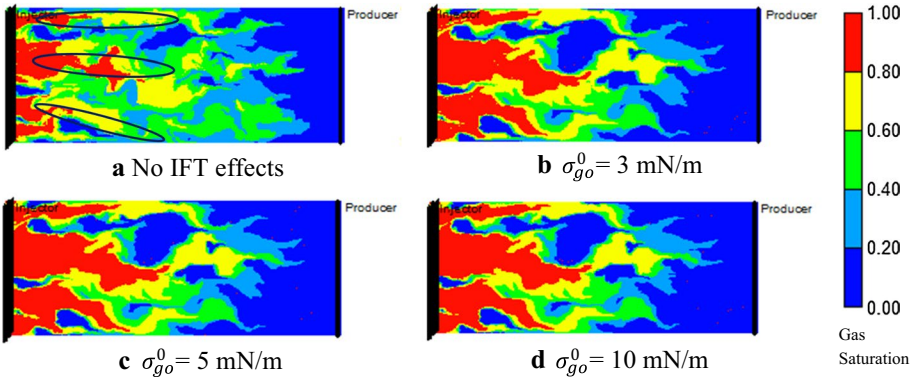

Fig. 13 Gas saturation after 0.5 PVI of CO_2 at near-miscible conditions

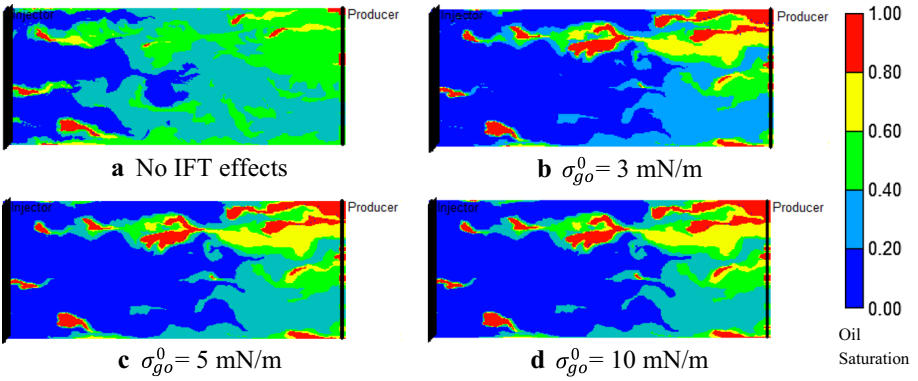

Fig. 14 Remaining oil saturation after 1 PVI near-miscible displacement

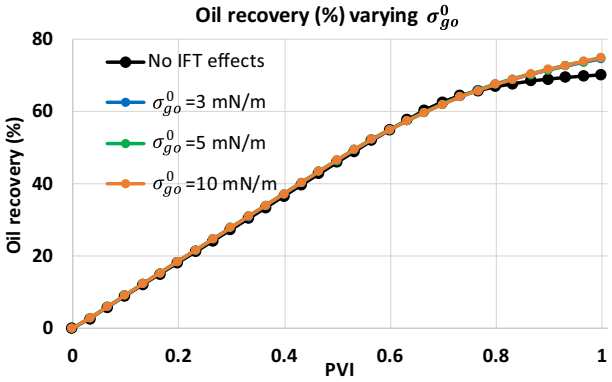

Fig. 15 Oil recovery after 1 PVI varying the threshold value at near-miscible conditions

much higher in the near-miscible case than in the immiscible case in the preferential routes (as indicated by the oval shapes). At near-miscible conditions, the oil components have been mostly vaporized into the CO_2 and thus flow in the gas phase. As a result, the greatly increased gas saturation will form more aggressive gas fingers at near-miscible conditions than at immiscible conditions. Note that the reduction in oil viscosity is minor in our case (see Fig. 32 in Appendix). In other words, the flow is unstable during the whole injection process. More interestingly, IFT effects mobilize some oil, which leads to an even worse macroscopic sweep efficiency. Both mechanisms are working in tandem to recover the oil in the preferential routes (as indicated by the oval shapes) but forming more severe gas fingers at the same time, as seen in Fig. 13a–d. As a result, the oil in the preferential routes can be more efficiently produced, whereas the oil in the non-preferential routes is even more poorly recovered than in the base case (Fig. 14). The results in Fig. 15 show that the oil recovery after 1 PVI has been modestly increased by the IFT effects, but only by a limited amount due to viscous instability forming dominant gas fingers. This case with continuous CO_2 injection also shows that there is a significant amount of bypassed oil in the non-preferential routes.

4.5 2D Areal Test: 2 PVI WAG CO_2 Injection at Near-Miscible Conditions (120 bar)

We now address the issue of the oil left in the non-preferential routes which is left because of the overall impact of the IFT effects leading to such dominant gas fingers. The analysis of these interactions between oil stripping/compositional effects (M_{CE}) and IFT effects (M_{IFT}) has led us to consider WAG injection, which is expected to improve the stability of the displacing front. Therefore, a range of numerical simulations of near-miscible WAG displacement with the aforementioned injection strategy (Table 1) were conducted with/without IFT effects as shown in the following. At this stage, Stone 2 was selected to produce the 3PRP in our simulations, but a further sensitivity analysis of the 3PRP models is presented in the next section.

Figure 16 shows the remaining oil saturation at various stages of the WAG simulations comparing near-miscible cases both with and without the IFT effects included. The figures on the left (a–d) show the results without IFT effects, and those on the right (e–h) with IFT effects. As expected, WAG is able to efficiently improve macroscopic sweep in both cases. Very importantly, the displacement performance has been significantly enhanced in the case including IFT effects, particularly in the non-preferential routes. Eventually, there

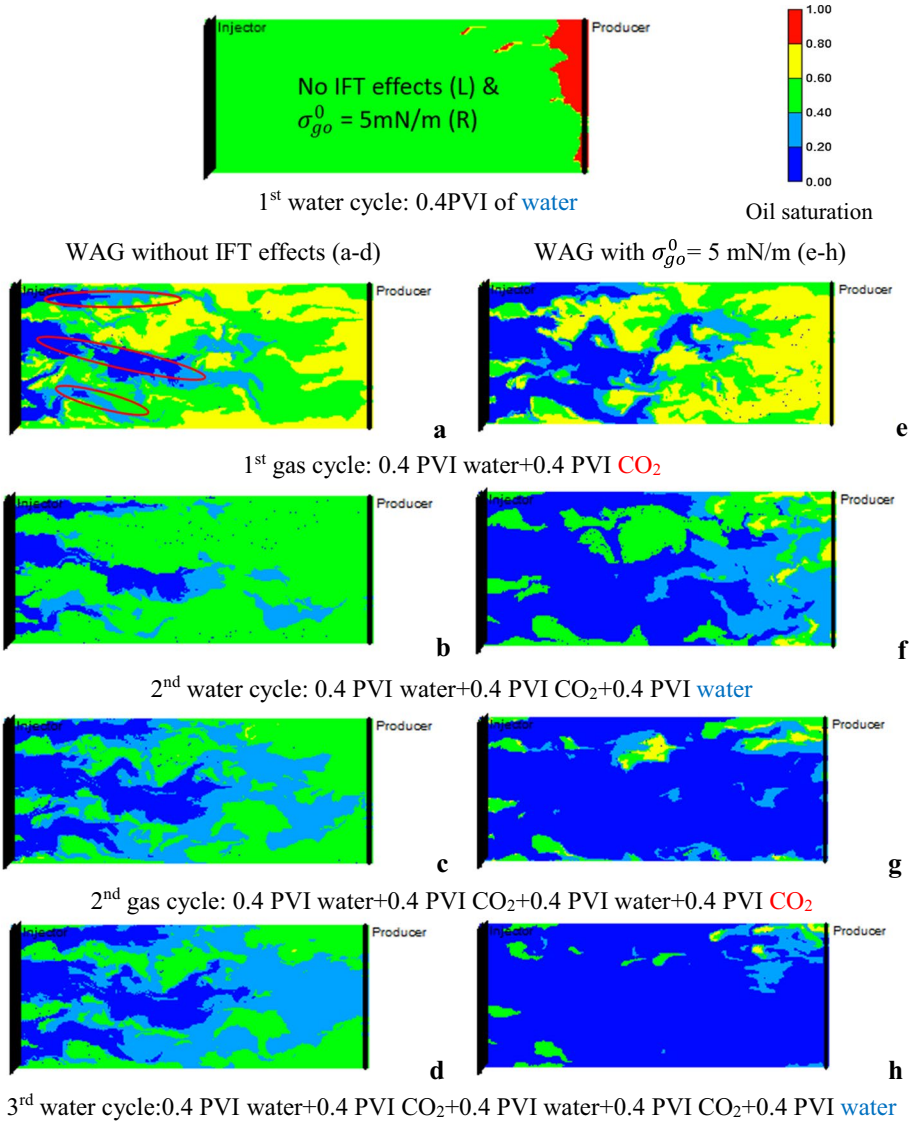

Fig. 16 Track of remaining oil saturation throughout the 2 PVI of WAG

has been a very significant increase (17%) on the ultimate oil recovery as shown in Fig. 17. It is very evident that this improvement has come from the much improved sweep of the non-preferential (bypassed) flow paths.

We now address the question: how do IFT effects significantly improve the displacement performance in non-preferential routes? Either the gas fingers are redistributed and strip the oil again (oil components recovered via the "gas" phase through mechanism, M_{CE}), or oil is greatly mobilized and produced as the mobile oil phase (through mechanism, M_{IFT}). To answer this question, we select two representative cells (3/10 of the system

length from the injector) shown in Fig. 18, one in a preferential route (indicated as a square shape) and the other in a non-preferential route (indicated as a triangular shape). We analysed the parameters of phase flow velocity and interfacial tension throughout the whole injection process for these two cells. (Several pairs of cells were studied but results for just one typical pair is presented here.)

As seen in Fig. 19a, b, the oil velocity out of the cell in the non-preferential route has been greatly increased by the IFT effects during the first gas cycle (0.4–0.8 PVI) and in particular the second water cycle (0.8–1.2 PVI). In contrast to the oil stripping effects (M_{CE}), the IFT effect (M_{IFT}) is not dependent on continuous contact between oil and CO_2. Instead, the remaining oil is mobilized by IFT relative permeability effects and can be efficiently produced by the subsequent water injection. As a result, the most incremental recovery is from the second water cycle compared with the base case without IFT effects (Fig. 20).

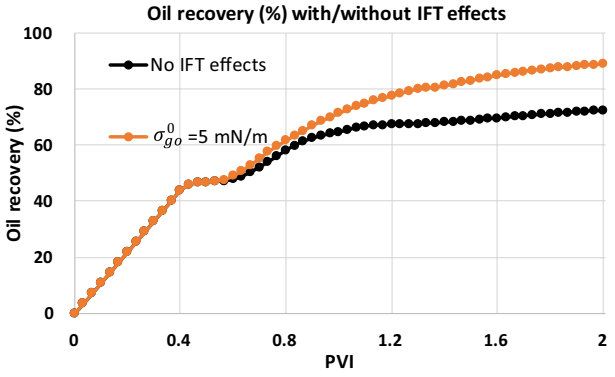

Fig. 17 Oil recovery with/without the account of IFT effects

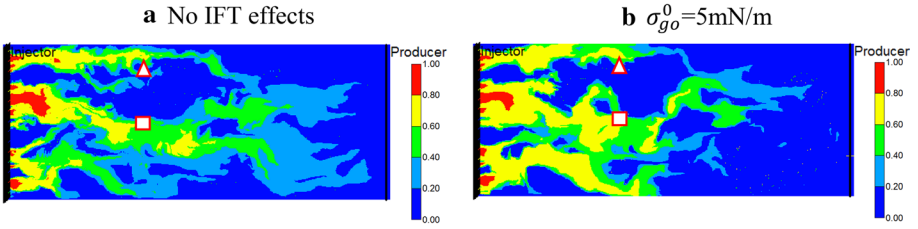

Fig. 18 Gas saturation at the end of first gas injection cycle: no IFT effects (*L*) and σ^0_{go} = 5 mN/m (*R*)

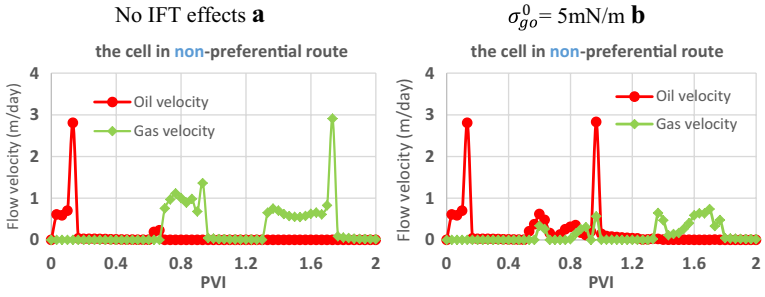

Fig. 19 Phase velocity out of the cell in the non-preferential route

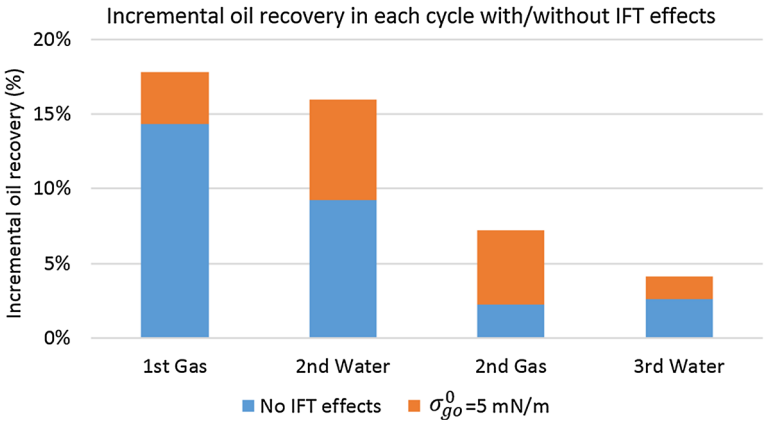

Fig. 20 Incremental oil recovery in each cycle

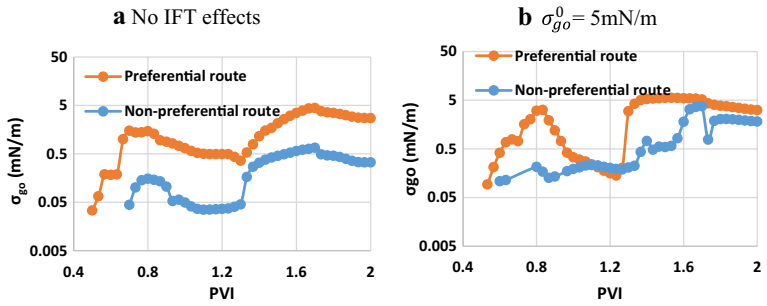

Fig. 21 Comparison of the σ_{go} in the representative cells throughout the injection

Moreover, there has been no increase in the gas velocity in the cell in the non-preferential route, which further indicates that the improved oil displacement performance is mainly a result of the IFT effects (M_{IFT}) rather than stripping effects (M_{CE}). In a later paper, we will demonstrate that this improvement in oil recovery from the non-preferential paths is due to a local viscous crossflow mechanism which is prevalent during the water cycle following the gas cycle (Wang et al. 2019b).

We also found that the magnitude of σ_{go} in the preferential route was generally greater than in the non-preferential route. This is because of the fact that the two cells are at unequal stages of oil stripping effects, i.e. the preferential route is at a later stage than the non-preferential route (Fig. 21). For this reason, the incremental oil mobility due to IFT effects is much less in the preferential route than in the non-preferential route. Besides that, the local displacement performance is already very efficient in the preferential route even without the IFT effects. As seen in Fig. 22a, b, there has been only a minor increase in the oil velocity during the first gas cycle (0.4–0.8 PVI) and no evident increase has been observed during the rest of the injection. Therefore, we conclude that IFT effects have presented very limited impact in the preferential routes, particularly when oil stripping effects are dominant. This further demonstrates why continuous gas injection without WAG is less efficient than applying near-miscible WAG. See also the further discussion in Wang et al. (2019b).

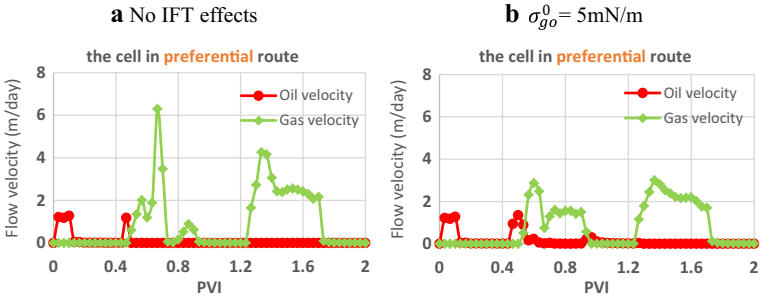

Fig. 22 Phase velocity out of the cell in the preferential route

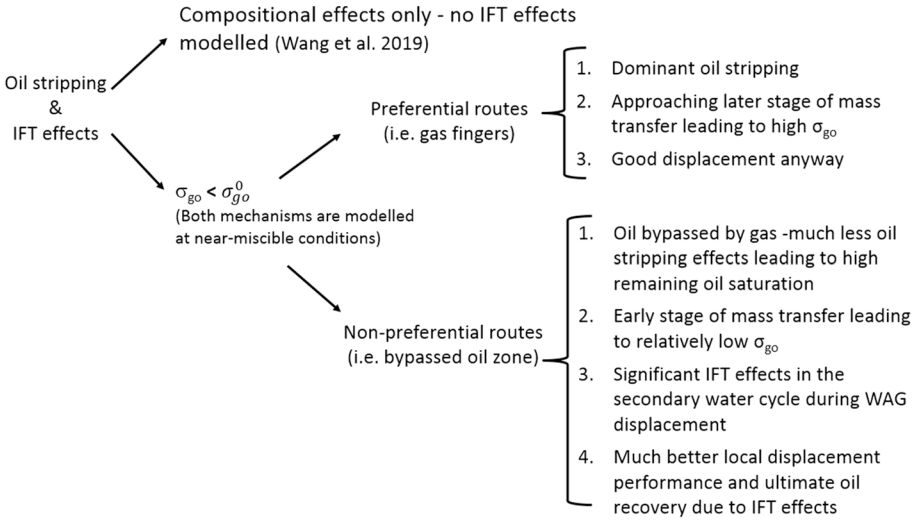

Fig. 23 Summary map of the main findings from our study

Results in Figs. 19 and 22 show that the gas velocity in the cells of both preferential and non-preferential routes is reduced when IFT effects are included. This is because oil has been mobilized at high gas saturation (K_{rg} close to 1), leading to a reduction in the gas relative permeability at the same time (Fig. 3). It is concluded that IFT effects can greatly enhance the local displacement performance with WAG injection in non-preferential (bypassed) flow routes and thus improve the ultimate oil recovery. Together with the results from our previous paper (Wang et al. 2019a), we show a summary map of our findings so far (Fig. 23).

4.6 2D Areal Test: Sensitivity Analysis of the 3PRP Methods on Flow Behaviour

It is well known that the result of a gas injection can be greatly influenced by the choice of 3PRP model. For this reason, a sensitivity analysis of three of the most widely used 3PRP models was performed, namely Stone 1, Stone 2 and Baker's saturation-weighted method. Figure 24 shows the distribution of remaining oil saturation after 2PV near-miscible WAG

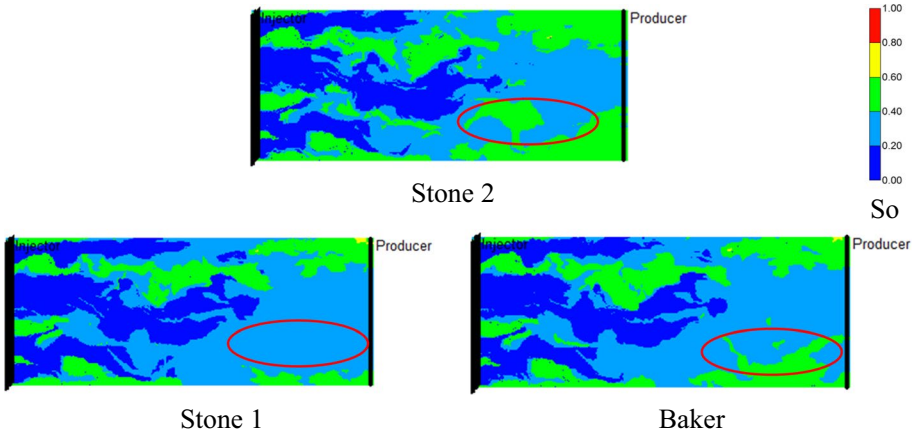

Fig. 24 Remaining oil saturation varying 3PRP methods without IFT effects

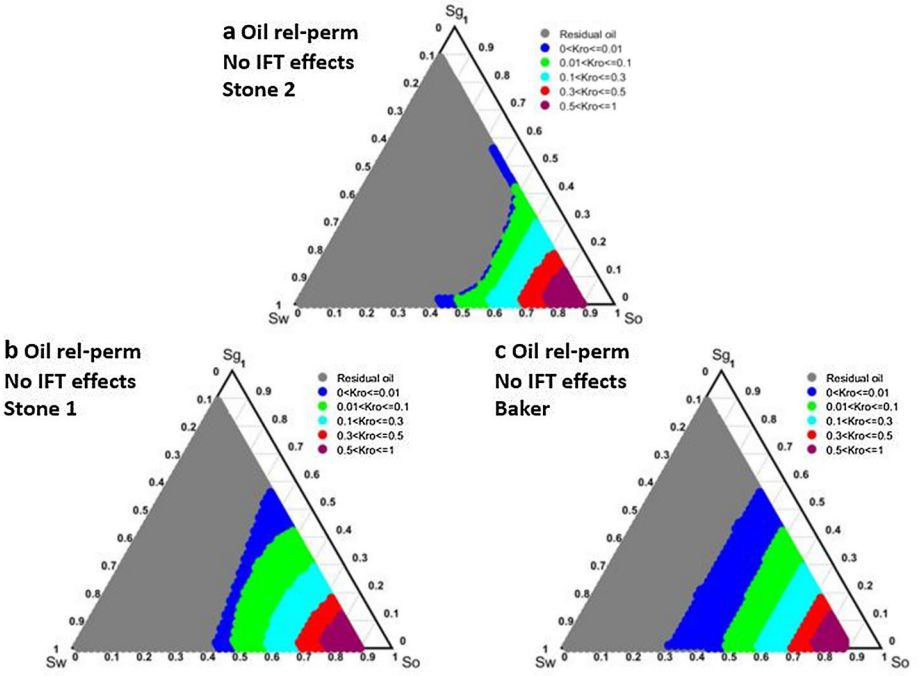

Fig. 25 Oil isoperm varying 3PRP methods: **a** Stone 2, **b** Stone 1, **c** Baker

displacement in the absence of IFT effects. As seen in Fig. 24, the only observable differences are mainly in the area of the non-preferential routes, particularly near the producer. There is less remaining oil in the area indicated by red oval with the Stone 1 model than with the other two models.

Figure 25a–c presents three sets of oil isoperms produced from each of these methods. The main differences between these models are in the region approaching residual

oil saturation (as expected). Stone 2 has the largest area of residual oil saturation, whereas Stone 1 has the smallest. As a result, Stone 2 gives the most pessimistic prediction in terms of oil recovery, whereas Stone 1 gives the most optimistic prediction, although these differences are relatively modest as shown in Fig. 26. Clearly, the Stone 2 recovery result is not a "prediction", it is essentially "input", as no simulation needs to be done to reach this conclusion. However, the residual oil saturation in this ternary diagram can be significantly overcome by compositional effects in near-miscible gas injection to achieve a much lower remaining oil saturation. In other words, oil components can be vaporized into CO_2 and produced in the "gas" phase (supercritical fluid, in fact, but using gas relative permeability for flow velocity), particularly from the preferential routes where oil stripping effects can be dominant. This is also the reason why there are only observable discrepancies in the non-preferential routes when using different 3PRP models.

The results in Fig. 27 now show the distributions of remaining oil saturation after 2PV near-miscible WAG displacement including IFT effects. Interestingly, these results show that the discrepancies have been much reduced.

The question now is how do IFT effects influence the oil isoperm and reduce the discrepancies of results when varying 3PRP methods. Here, we present two examples of

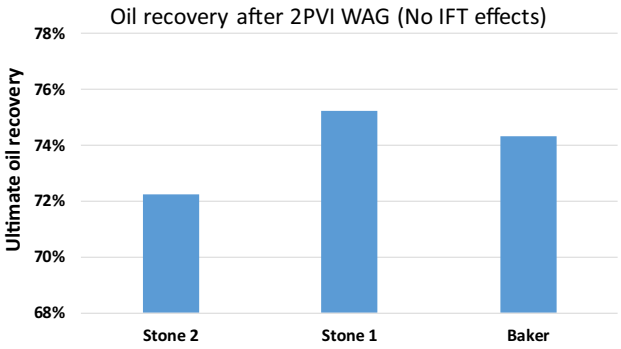

Fig. 26 Ultimate oil recovery varying 3PRP methods without IFT effects

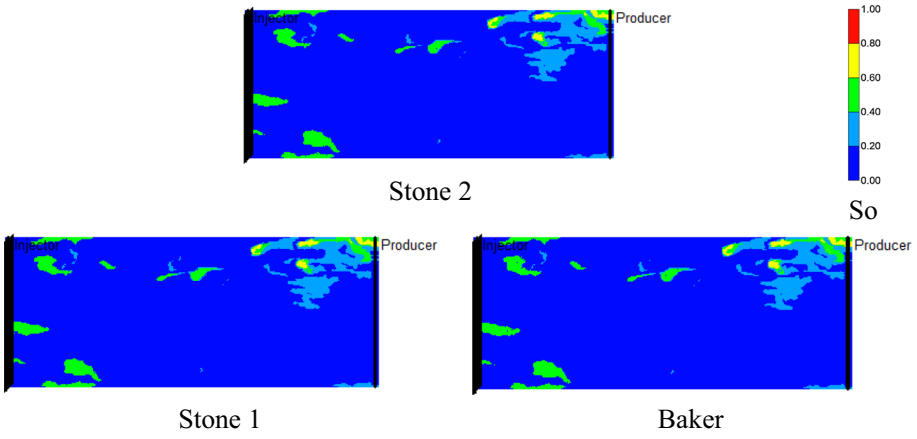

Fig. 27 Remaining oil saturation varying 3PRP methods with IFT effects

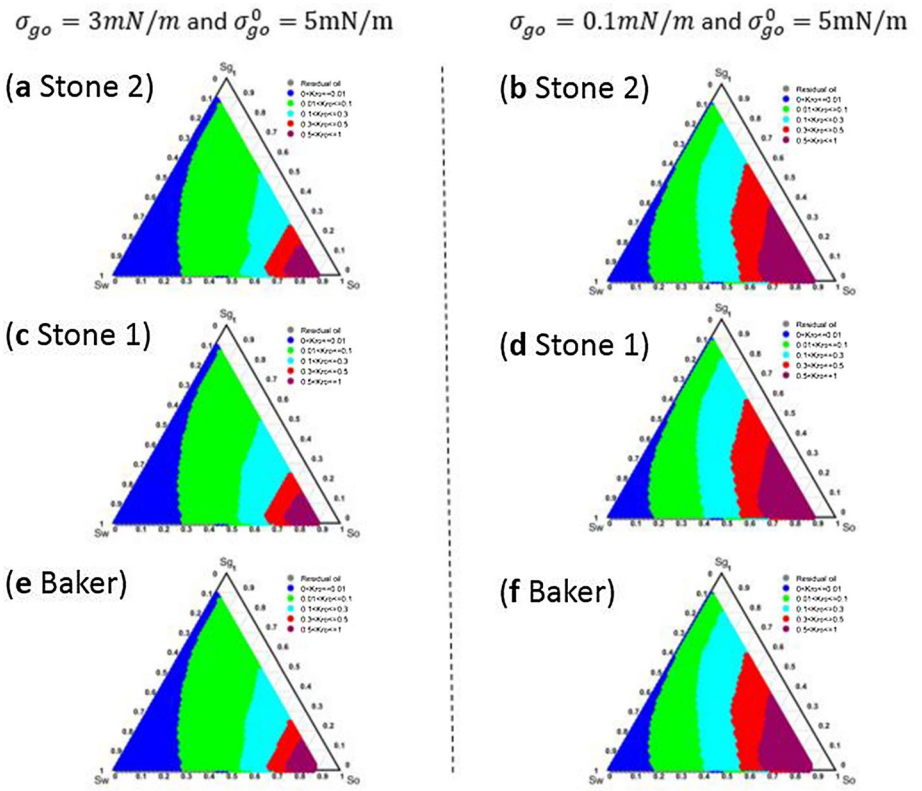

Fig. 28 Oil isoperm varying 3PRP methods: **a**, **b** Stone 2, **c**, **d** Stone 1 and **e**, **f** Baker with IFT effects

relative permeability varying the ratio of σ_{go} (3 mN/m and 0.1 mN/m) and threshold value ($\sigma^0_{go} = 5$ mN/m). As seen in Fig. 28, the oil isoperm diagrams are becoming much more similar with decreasing σ_{go}. This is because of the nature of the method used for modelling IFT effects which we have applied (Eq. 1–4). This method entails an interpolation between immiscible (initial) and miscible relative (K_{rh}) permeabilities, under the control of a weighting factor (Eq. 4). The lower σ_{go}, the lower the contribution which the initial 3PRP can make to the final oil relative permeability. In other words, the oil relative permeability should be almost the same regardless of the modelling method at certain local values of σ_{go}, such as at the ultra-level (0.001 mN/m). As expected, the results in Fig. 29 show that there is hardly any difference in the prediction of the ultimate oil recovery.

5 Summary and Conclusions

The central objective of this paper is to study the balance and interactions of the different mechanistic contributions to the physics occurring during oil displacement by CO_2 (both in continuous gas injection and in WAG). Mechanism 1 (M_{CE}) is the conventional

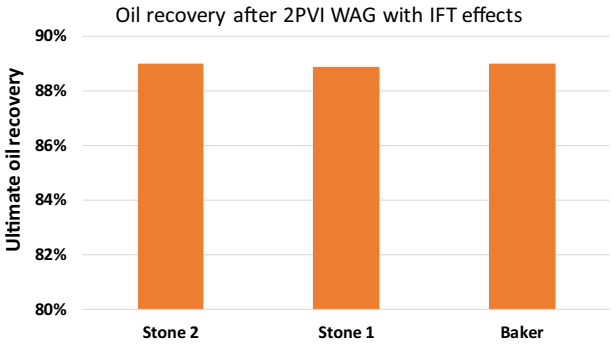

Fig. 29 Ultimate oil recovery varying 3PRP methods with $\sigma^0_{go} = 5$ mN/m

oil stripping/compositional effect, and Mechanism 2 (M_{IFT}) is the near-miscible IFT effect on oil relative permeability through enhanced layer flow. We have studied how these M_{CE} and M_{IFT} mechanisms operate in a heterogeneous permeability field. Using sufficiently fine-scale models, we explain how these mechanisms interact with each other and affect the sweep and local displacement efficiency. We believe that studying the key processes both separately and together leads to a greater insight into the physics of CO_2 displacement, and this will help us to simulate the transition from immiscible to miscible displacement consistently at larger scales. By performing simulations of CO_2 injection in 2D systems, we make five observations of how both the compositional (M_{CE}) and IFT (M_{IFT}) effects influence the flow behaviour.

1. Incremental oil recovery is insensitive to IFT effects during continuous CO_2 injection. This is because both M_{CE} (oil stripping effects) and M_{IFT} (IFT effects) are working in tandem to recover the oil in the preferential routes, but forming more severe gas fingers at the same time leading to more imbalanced flow paths. The final result of the competing IFT effects of poorer sweep but lower residual oil in the preferential paths leads to a very limited increased oil recovery.
2. Our simulations confirm that WAG is able to make better use of IFT effects than continuous injection, particularly in the non-preferential flow routes. Unlike stripping effects (M_{CE}), IFT effects are not dependent on continuous contacts between CO_2 and oil. Instead, the remaining oil could be mobilized by IFT effects and be efficiently recovered by the subsequent water injection. As a result, the most incremental recovery is achieved during the second water cycle, which contrasts with the base case without IFT effects. In the forthcoming paper, we demonstrate a local viscous crossflow mechanism is operating at each water injection stage of the WAG cycle (Wang et al. 2019b). This causes oil to crossflow (by enhanced film-flow effects in the hydrocarbon 3PRP) from the non-preferential region into the main preferential flow pathway (gas fingers) from which the oil is produced relatively quickly.

3. Note that the magnitude of the impacts that IFT effects could have on the fluid behaviour is greatly dependent on the stage of mass transfer between CO_2 and oil. The IFT decreases initially, but it increases later as a result of leaving most of heavier components in the remaining oil. For this reason, it is particularly important to include the heavy ends of the oil composition to properly reflect this process and the combined outcome from the interactions of both mechanisms. A very simple oil EOS with too few components would omit this potentially important effect.
4. Slim-tube tests (100% sweep and homogenous) yield pessimistic predictions as to the possible improvement in displacement performance due to the IFT effects (M_{IFT}). On the other hand, slim-tube tests tend to overestimate the improved oil recovery through oil stripping effects (M_{CE}), according to our previous study (Wang et al. 2019a).
5. In this work, we have presented a new analysis of the processes occurring during the transition from immiscible to miscible displacement. The key findings describe how different mechanisms (oil stripping, M_{CE} and IFT effects, M_{IFT}) work in different parts of a model (preferential and non-preferential routes), and for different processes (continuous CO_2 injection and WAG) at different conditions (immiscible and near miscible).

Acknowledgements The authors would like to gratefully acknowledge the funding for this study by the sponsor of the "Best in Class Predictions of Enhanced Oil Recovery Using CO_2 Injection" project at Heriot-Watt University (Petronas and Uzma). Energi Simulation is thanked for funding the chair in Reactive Flow Simulation at Heriot-Watt University held by Eric Mackay. We also thank Professor Arne Skauge of U. Bergen, Norway, for many helpful discussions on the physics and modelling of WAG displacements.

Appendix

(See Figs. 30, 31, 32.)

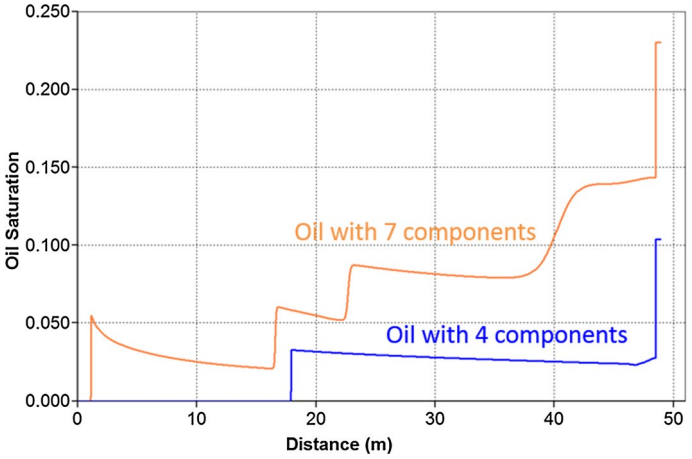

Fig. 30 Oil saturation along the slime tube after 1PV continuous CO_2 injection under near-miscible conditions using four-component and seven-component pseudo-oil

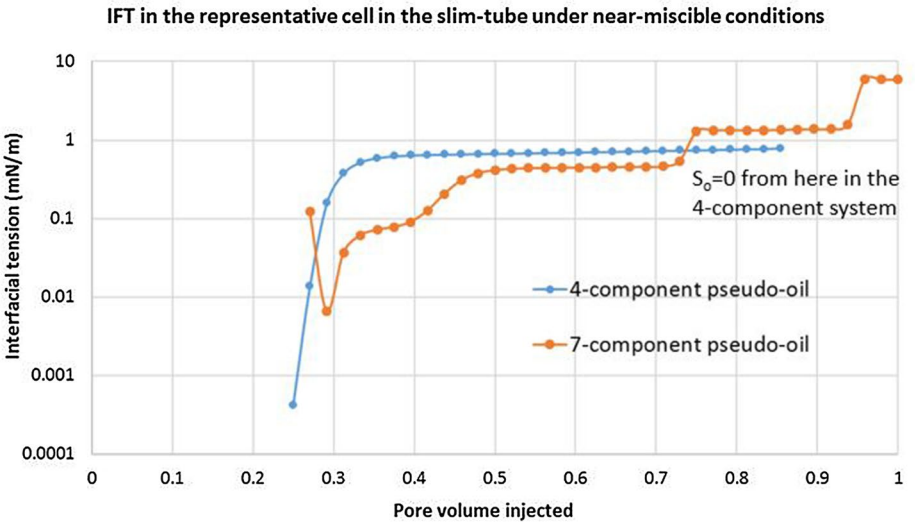

Fig. 31 Oil–gas interfacial tension of a representative cell with continuously injected pore volume of CO_2 under near-miscible conditions using four-component and seven-component pseudo-oil

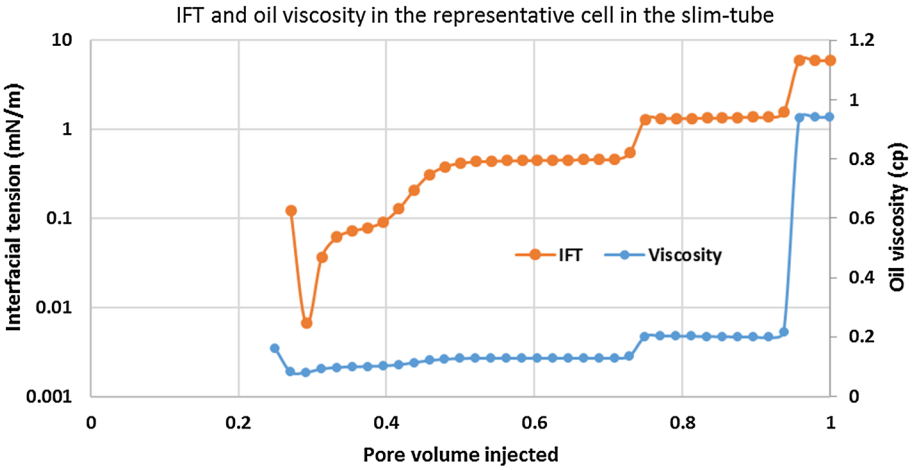

Fig. 32 Oil viscosity and the IFT during the whole injection process in the representative of the slim tube for the seven-component system

References

Al-Siyabi, Z., Danesh, A., Tohidi, B., Todd, A.: Variation of gas–oil–solid contact angle with interfacial tension. Pet. Geosci. **5**(1), 37–40 (1999)

Amaefule, J.O., Handy, L.L.: The effect of interfacial tensions on relative oil/water permeabilities of consolidated porous media. Soc. Pet. Eng. J. **22**(03), 371–381 (1982)

Aziz, K., Settari, A.: Petroleum Reservoir Simulation (476). Applied Science Publ. Ltd., London (1979)

Baker, L.: Three-phase relative permeability correlations. In: SPE Enhanced Oil Recovery Symposium. Society of Petroleum Engineers (1988)

Bardon, C.: Gas/oil relative permeabilities and residual oil saturations in a field case of a very light oil, in the near-miscibility conditions. In: SPE Annual Technical Conference and Exhibition. Society of Petroleum Engineers (1994)

Betté, S., Hartman, K.J., Heinemann, R.F.: Compositional modeling of interfacial tension effects in miscible displacement processes. J. Pet. Sci. Eng. **6**(1), 1–14 (1991)

Blunt, M.J.: An empirical model for three-phase relative permeability. Soc. Pet. Eng. J. **5**(04), 435–445 (2000)

CMG: CMG-GEM technical manual, Computer Modelling Group (2017)

Coats, K.H.: An equation of state compositional model. Soc. Pet. Eng. J. **20**(05), 363–376 (1980)

Dykstra, H., Parsons, R.: The prediction of oil recovery by waterflood. Sec. Rec. Oil U. S. **2**, 160–174 (1950)

Green, D.W., Willhite, G.P.: Enhanced oil recovery. Richardson, Tex.: Henry L. Doherty Memorial Fund of AIME, Society of Petroleum Engineers (1998)

Jahanbakhsh, A., Shahverdi, H., Fatemi, S., Sohrabi, M.: Gas/oil IFT, three-phase relative permeability and performance of water-alternating-gas (WAG) injections at laboratory scale. J. Oil Gas Petrochem. Sci. **1**(1), 00005 (2018)

Journel, A.G., Huijbregts, C.J.: Mining Geostatistics, vol. 600. Academic press, London (1978)

Juanes, R., Spiteri, E. J., Orr, F. M. and Blunt, M. J. (2006) 'Impact of relative permeability hysteresis on geological CO2 storage', *Water Resources Research*, 42(12)

Longeron, D.G.: Influence of very low interfacial tensions on relative permeability. Soc. Pet. Eng. J. **20**(05), 391–401 (1980)

Orr, F.M.: Theory of Gas Injection Processes. Tie-Line Publications, Copenhagen (2007)

Schlumberger: Eclipse technical manual, Schlumberger Limited (2015)

Shyeh-Yung, J.: Mechanisms of miscible oil recovery: effects of pressure on miscible and near-miscible displacements of oil by carbon dioxide. In: SPE Annual Technical Conference and Exhibition. Society of Petroleum Engineers (1991)

Sohrabi, M., Danesh, A., Jamiolahmady, M.: Visualisation of residual oil recovery by near-miscible gas and SWAG injection using high-pressure micromodels. Transp. Porous Media **74**(2), 239–257 (2008a)
Sohrabi, M., Danesh, A., Tehrani, D.H., Jamiolahmady, M.: Microscopic mechanisms of oil recovery by near-miscible gas injection. Transp. Porous Media **72**(3), 351–367 (2008b)
Sohrabi, M., Tehrani, D., Danesh, A., Henderson, G.: Visualization of oil recovery by water-alternating-gas injection using high-pressure micromodels. Soc. Pet. Eng. J. **9**(03), 290–301 (2004)
Sorbie, K.S., van Dijke, M.I.J.: The mechanism of oil recovery by water-alternating-gas injection at near-miscible conditions in mixed wet systems. In: SPE Improved Oil Recovery Symposium. Society of Petroleum Engineers (2010)
Stalkup, F.I.: Miscible Displacement, vol. 8. Dallas, Texas (1983)
Tang, D., Zick, A.: A new limited compositional reservoir simulator. In: SPE Symposium on Reservoir Simulation. Society of Petroleum Engineers (1993)
Wang, G., Pickup, G.E., Sorbie, K.S., Mackay, E.J.: Analysis of compositional effects on global flow regimes in CO_2 near-miscible displacements in heterogeneous systems. Transp. Porous Media **129**, 743–759 (2019a)
Wang, G., Pickup, G.E., Sorbie, K.S., Mackay, E.J., Skauge, A.: Analysis of near-miscible CO_2-WAG displacements: the distinction between compositional and interfacial tension effects SPE-193907. In: SPE Reservoir Simulation Conference. Society of Petroleum Engineering (2019b)
Zick, A.: A combined condensing/vaporizing mechanism in the displacement of oil by enriched gases. In: SPE Annual Technical Conference and Exhibition. Society of Petroleum Engineers (1986)

Affiliations

Gang Wang[1] · Gillian E. Pickup[1] · Kenneth S. Sorbie[1] · Eric J. Mackay[1]

✉ Gang Wang
Gw72@hw.ac.uk

Gillian E. Pickup
G.Pickup@hw.ac.uk

Kenneth S. Sorbie
K.Sorbie@hw.ac.uk

Eric J. Mackay
E.J.Mackay@hw.ac.uk

[1] Heriot-Watt University, Edinburgh, UK